PROCEEDINGS, TOUGH Symposium 2003
Lawrence Berkeley National Laboratory, Berkeley, California, May 12–14, 2003

MODELING STUDIES OF MOUNTAIN-SCALE RADIONUCLIDE TRANSPORT IN THE UNSATURATED ZONE AT YUCCA MOUNTAIN, NEVADA

George J. Moridis, Yongkoo Seol, and Yu-Shu Wu

Lawrence Berkeley National Laboratory, 1 Cyclotron Rd., ESD, MS90-1116, Berkeley, CA 94720, U.S.A.
e-mail: GJMoridis@lbl.gov, Yseol@lbl.gov, YSWu@lbl.gov

ABSTRACT

We investigate radionuclide transport from a high-level nuclear waste repository to be situated in the unsaturated zone (UZ) at Yucca Mountain (YM), Nevada. Several radioactive solutes (that cover the range of sorption behavior) and colloids of various sizes are studied. The results of the study indicate the importance of the subsurface geology and site hydrology, i.e., the presence of faults (they dominate and control transport), fractures (the main migration pathways), and the relative distribution of zeolitic and vitric tuffs. The effects of the climatic conditions, diffusion, and sorption (for solutes) or infiltration (for colloids) onto the matrix are discussed. The influence of the colloid size on transport is also investigated.

INTRODUCTION

The U.S. Department of Energy (DOE) is actively investigating the technical feasibility of permanent disposal of high-level nuclear waste in a repository to be situated in the unsaturated zone (UZ) at Yucca Mountain (YM), Nevada. The proposed site is located in southern Nevada about 120 km northwest of Las Vegas. The attractive attributes of the site include a semi-arid climate with an average rainfall of about 170-190 mm/yr (indicating low infiltration rates through the potential repository), a thick UZ (600-700 m), the presence of rocks onto which important radionuclides in the wastes tend to sorb strongly, and the relative isolation and sparse population of the proposed area.

The YM stratigraphy consists of layers of welded and nonwelded tuffs with vastly different hydraulic properties (Montazer and Wilson, 1984). The location of the proposed repository is approximately 300 m below the surface, i.e., at the midpoint between the surface and the water table (Dyer and Voegele, 19960.

The purpose of this study is to evaluate by means of 3-D numerical modeling the transport of radioactive tracers (solutes and colloids) in the UZ under ambient conditions from the potential repository horizon to the water table at YM. The model considers the transport of radioactive colloids through fractured tuffs, and the effects of changes in the intensity and configuration of fracturing from hydrogeologic unit to unit. The results of the simulations are used to determine the relative importance of processes, mechanisms, and geologic features that significantly affect transport.

GEOLOGICAL MODEL AND PHYSICAL PROCESSES

The subsurface formation at YM consists of heterogeneous layers of anisotropic, fractured volcanic rocks. Beginning from the land surface downward, the YM geologic units are the Tiva Canyon, Yucca Mountain, Pah Canyon, and the Topopah Spring Tuffs of the Paintbrush Group. Underlying these are the Calico Hills Formation, and the Prow Pass, Bullfrog, and Tram Tuffs of the Crater Flat Group. These formations have been divided into major hydrogeologic units based roughly on the degree of welding. These are the Tiva Canyon welded (TCw); the Paintbrush nonwelded (PTn), consisting primarily of the Yucca Mountain and Pah Canyon members and the interbedded tuffs; the Topopah Spring welded (TSw); the Calico Hills nonwelded (CHn); and the Crater Flat undifferentiated (CFu) hydrogeologic units (Bodvarsson et al., 1999; Hinds and Pan, 2000).

Conceptual models of flow at YM are described in Liu et al. (2000). The site of the proposed repository is the TSw unit, and more specifically the tsw34, tsw35, and tsw36 layers of the UZ, depending on the location (Hinds and Pan, 2000; Liu et al., 2000). Unsaturated flow in the TSw is primarily through the fractures, because the matrix permeability is several orders of magnitude lower than that in the fractures. The CHn and the Prow Pass (PP) unit below the proposed repository horizon are complex geological systems, with highly heterogeneous distributions of fracture and matrix hydrological properties that are expected to have a pronounced effect on the transport of radionuclides in the UZ.

There is limited hydrologic and transport information on the CHn unit and even less on the PP. The permeability of nonwelded tuffs is strongly dependent on the degree of alteration of the rock minerals into zeolites. Thus, based on the degree of zeolitic alteration, the CHn major hydrogeologic unit

is composed of vitric (CHv) and zeolitic (CHz) units (Hinds and Pan, 2000). Flow in the CHz units is expected to be concentrated in the fractures because of the large permeability contrast (about five orders of magnitud) between the matrix and the relatively permeable fractures (Liu et al., 2000). In nonwelded vitric tuffs such as the rocks in CHv units, the matrix and fracture permeabilities are on the same order of magnitude (Liu et al., 2000). Thus, these layers behave as porous (rather than fractured) media, and flow is matrix-dominated.

The CHz units are predominant in the northern part of the proposed repository, while the CHv units are concentrated in the southern part (Hinds and Pan, 2000). The areal distribution of the CHz and CHv units, and the corresponding fracture-matrix permeability contrast, have important implications for transport.

Fracture-dominated flow is associated with short contact times, limited radionuclide removal through diffusion and sorption, and thus transport over longer distances. Although radionuclides are more strongly adsorbed onto zeolitic units than onto vitric units, the fast fracture flow may not allow adequate matrix penetration and subsequent tracer retardation through sorption (in solutes) or filtration (in colloids). Conversely, the fracture-matrix permeability parity in the CHv units leads to longer contact times, and increased contaminant retardation through diffusion and sorption. These conditions lead to expectations of earlier (and in higher concentrations) arrival of radionuclides at the water table in the northern part of the proposed repository.

THE NUMERICAL MODEL

Two codes were used for the 3-D site-scale transport simulations in this study: EOS9nT (Moridis et al., 1999) and T2R3D (Wu et al., 1996), both of which are members of the TOUGH2 family of codes (Pruess, 1991).

EOS9nT can simulate water flow and transport of an arbitrary number *n* of non volatile tracers (solutes and/or colloids) in the subsurface. It first solves the Richards equation, which describes saturated or unsaturated water flow in subsurface formations, and obtains the flow regime. The *n* linearly independent transport equations (corresponding to the *n* solutes/colloids) are then solved sequentially. The transport equations account for (a) advection, (b) molecular diffusion, (c) hydrodynamic dispersion (with full 3-D tensorial representation), (d) kinetic or equilibrium physical and chemical sorption (linear, Langmuir, Freundlich, or combined), (e) first-order linear chemical reaction, (e) radioactive decay, (f) colloid filtration (equilibrium, kinetic or combined), and (g) colloid assisted solute transport. A total of *n*-1 daughter products of radioactive decay (or of a linear, first-order reaction chain) can be tracked.

EOS9nT includes two types of Laplace transform formulations of the tracer equations, in addition to conventional timesteping. The Laplace transform is applicable to steady-state flow fields and allows a practically unlimited time step size and more accurate solution (as numerical diffusion is significantly reduced).

T2R3D (Wu et al., 1996) simulates flow (saturated and/or unsaturated) and the coupled transport of a single radioactive solute tracer. The transport equations account for advection, molecular diffusion, hydrodynamic dispersion and linear equilibrium sorption.

The grid for this 3-D study of UZ transport was the same in the EOS9nT and the T2R3D simulations, and consisted of 245,000 elements. A 2-D cross section (plan view) of the grid at the proposed repository level is shown in Figure 1.

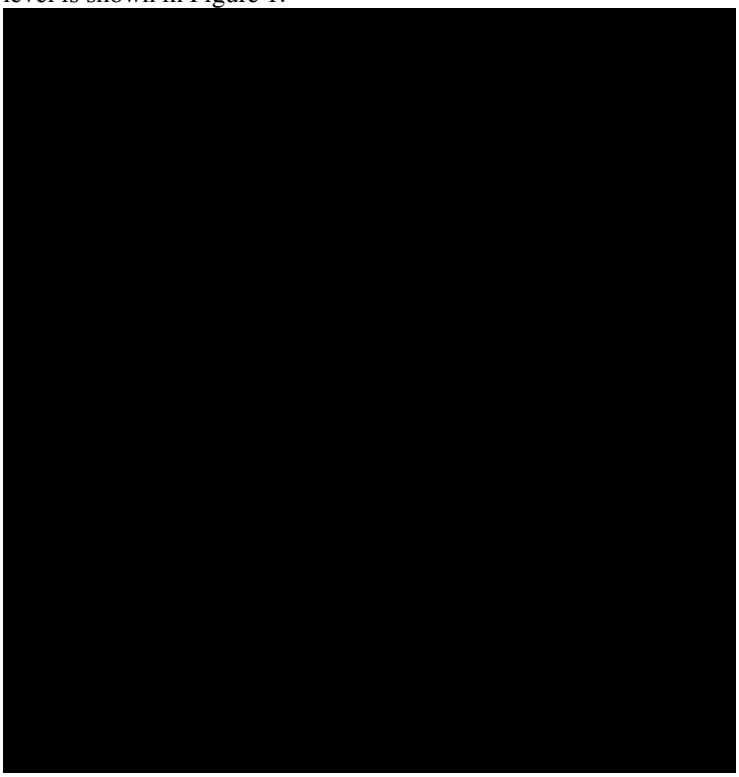

Figure 1. Plan view of the UZ model grid design at the proposed repository level

A dual-permeability conceptualization was used to describe the fracture-matrix system in the UZ (Wu et al., 2000). The diffusion, sorption and infiltration parameters for these studies can be found in Moridis et al. (2000). The radioactive species were released directly into the fractures of the elements corresponding to the proposed repository. We

investigated (a) instantaneous release, corresponding to a single catastrophic event, and (b) continuous release, describing a plausible long-term scenario involving the breaching of the waste-containing canisters and the slow discharge of their contents.

In the EOS9nT simulations, we employed Laplace transforms because of (a) the steady-state flow fields and (b) the assumption of linear solute sorption and colloid filtration. Because of its superior accuracy (especially in the solution of the transport of daughters), the method of DeHoog et al. (1982) was used for the Laplace-based solutions.

TRANSPORT OF ^{99}Tc, ^{237}Np, AND ^{239}Pu – INSTANTANEOUS RELEASE

These three radionuclides were studied because (a) they are expected to be present in large quantities in the isolated waste, (b) they have long half-lives, and (c) they represent the range of expected sorption behavior in the UZ (^{99}Tc is non-sorbing, ^{237}Np is moderately sorbing, and ^{239}Pu sorbs strongly).

There are two possible mechanisms of radionuclide removal and retardation in the transport of these substances: diffusion into the matrix through the fracture walls, and sorption. The results of the T2R3D simulations are shown in the YM water table breakthrough curves of Figures 2, 3 and 4 (for ^{99}Tc, ^{237}Np and ^{239}Pu, respectively) for three-levels of present-day infiltration (low, mean, and high).

Figures 2, 3 and 4 show the dependence of transport on the infiltration regime. Thus, an increasing level of infiltration results in a faster transport to the water table. As expected, the travel times to the water table increase with the sorption affinity of the radionuclide. Diffusion is critically important in non-sorbing species such as ^{99}Tc (because it is the sole retardation process), but its role becomes progressively less pronounced as sorption increases. The breakthrough curves in Figures 2 to 4 reveal that the maximum attainable level of normalized mass fraction (denoting the ratio of the mass that crosses the bottom UZ boundary to the total mass released at the repository) depends on the infiltration regime. Thus, more humid climatic conditions have higher maxima because of faster travel times to the YM water table, resulting in shorter residence times in the UZ and, consequently, limited radioactive decay.

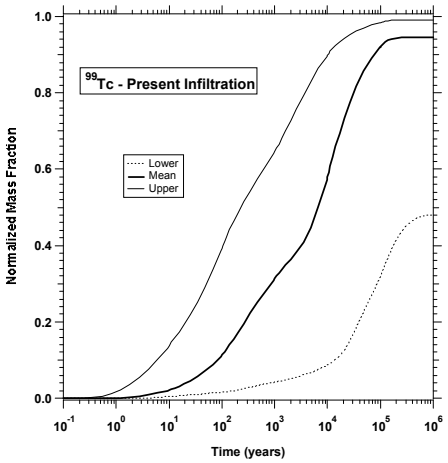

Figure 2. ^{99}Tc breakthrough at the YM water table after an instantaneous release.

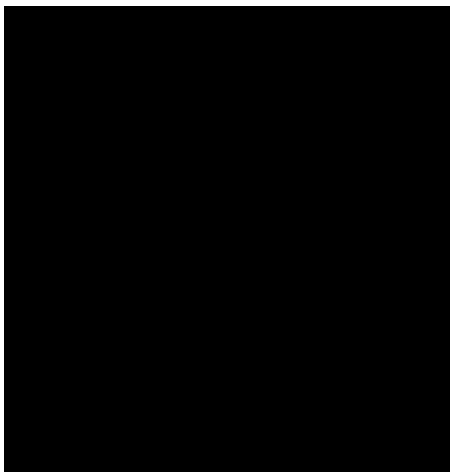

Figure 3. ^{237}Np breakthrough at the YM water table after an instantaneous release.

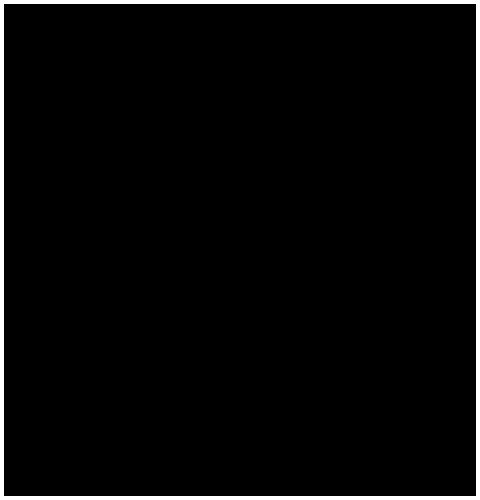

Figure 4. ^{241}Pu breakthrough at the YM water table after an instantaneous release.

The breakthrough curve of ^{239}Pu is noteworthy in that it exhibits two plateaus. The first is attributed to fast fracture flow (and the corresponding fast advection of ^{239}Pu to the water table), while the second plateau denotes matrix flow. The advent of matrix-related transport is less well defined in ^{237}Np, and cannot be discerned in the case of ^{99}Tc. Note the rather early arrivals of substantial fractions of the released ^{99}Tc and ^{237}Np mass at the water table, which occur at times considerably shorter than the radionuclide half-lives. Conversely, only a very small portion of the released ^{239}Pu mass ever reaches the water table because of its very strong sorbing affinity in the UZ matrix following diffusion through the fractures.

The large early radionuclide arrivals at the YM water table are attributed to the release approach (which places radionuclides in the fractures of all repository gridblocks, including those belonging to the highly conductive UZ faults) and the very fast fracture flow (and, consequently, advective transport) in the fault fractures. This is supported by the contour plot of the relative mass fraction (defined as the ratio of the radionuclide mass fraction to the initial mass fraction at the time of release) in the fractures at the YM water table in Figure 5. Even at the verly time of t = 10 years, the ^{99}Tc distribution at the water table (about 300 m below the repository) casts a strong signature and clearly delineates the fractures of the most important faults: the Drillhole Wash fault, and Pagany Wash fault, followed by the less important Sever Wash fault and the Sundance fault (Figure 1).

The pattern persists at t = 100 years (Figure 6), which further confirms the observation the transport is both dominated and controlled by the faults. Note that the fault signature is fainter at this time because the easily transportable radionuclide has already reached the water table, and the new arrivals are increasingly depleted in ^{99}Tc. Comparison to the corresponding matrix distribution in Figure 7 confirms that faults are the main transport-facilitating geologic features, but shows that they limit lateral transport into the matrix (as attested to by the similarity of the footprints of the fracture and matrix distributions, indicating limited movement of the radionuclide into the matrix). This is caused by the fast fracture flow that limits the residence time in the fractures, and, consequently, diffusion into the matrix.

The very early arrivals are a direct consequence of radionuclide release directly into the fractures of the fault because the repository footprint is allowed to straddle the important faults identified by the transport patterns at the YM water table (Figure 1). The obvious implication is that such faults (and their immediate vicinity) should be avoided as radioactive waste storage areas in the proposed repository.

TRANSPORT OF ^{99}Tc, ^{237}Np, AND ^{239}Pu – CONTINUOUS RELEASE

Continuous release is a realistic scenario, given the mass of the the radioactive substances stored at the site, the expected deterioration of the canisters, and the planned closure of the proposed repository after the storage of the radioactive materials (thus preventing access and repairs that might inhibit continuous release).

Figure 5. ^{99}Tc relative mass fracture distribution in the fractures at the YM water table at t = 10 years after an instantaneous release.

Figure 6. ^{99}Tc relative mass fracture distribution in the fractures at the YM water table at t = 100 years after an instantaneous release.

Figure 7. ^{99}Tc relative mass fracture distribution in the matrix at the YM water table at t = 100 years after an instantaneous release.

Under a continuous release regime, the conventional breakthrough concept is inadequate, and a criterion of a relative system performance based on the relationship of inflow and outflows across the system boundaries is needed. Such a criterion provides a measure of the ability or capacity of the domain to accumulate radionuclide mass that enters its boundary at a given rate, and is just as important (if not more so) than the conventional breakthrough study that can only describe response to a finite mass release. Thus, under instantaneous releases, masses are compared, while in continuous release the relationship of fluxes is established. For a complete evaluation of the repository, performance under both release scenarios must be evaluated.

Thus, the breakthrough concept here is based on the normalized or relative release rate, which is defined as the ratio of the radionuclide mass flux at the groundwater boundary to that at the proposed repository boundary. For radioactive chains, the quantity in the denominator reflects the sum of the fluxes of all members in the release stream. For decaying release concentration, the denominator reflects the original radionuclide flux across the repository boundary.

In this study, the released radionuclides were assumed to undergo decay at the input points (boundaries), and represents a realistic scenario or release from stored nuclear waste. Only mean present-day infiltration was considered in these simulations. The grids, flow fields and conditions in these EOS9nT simulations were the same used in the instantaneous release study.

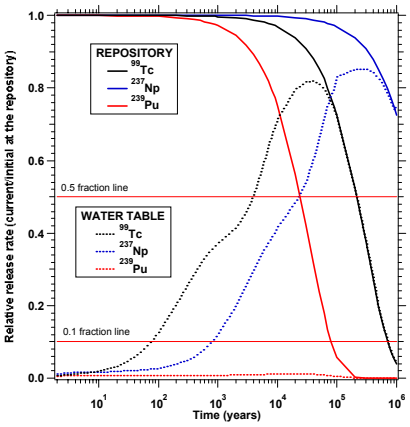

Figure 8. Normalized release rate of ^{99}Tc, ^{237}Np and ^{239}Pu at the YM water table for continuous release and mean present-day infiltration.

The breakthrough curves for continuously released ^{99}Tc, ^{237}Np and ^{239}Pu are shown in Figure 8, which also shows the decaying input fluxes (reflecting decaying concentrations, as the water fluxes remain time-invariant) for reference. These are consistent with the breakthrough curves for instantaneous release in Figures 2 to 4, although such agreement is not the rule. Of interest is the shape of the breakthrough curves, that begin to show a decline after reaching a maximum at the point of coincidence of the influx and outflow curves.

The existence of such a maximum is a direct consequence of considering a decaying source. The ratio of outflow to initial inflow initially increases as radionuclides reach the water table in increasing quantities. However, the increase can only proceed up to a point, beyond which there is a balance between influx and outflow (indicating by the coincidence of the two curves in Figure 8). Note that the maximum attainable normalized release rate for ^{239}Pu is much lower than the normalized mass fraction in Figure 4. This is because the flux to the water table boundary is small and increases slowly, and is much lower than the outflow at the repository.

TRANSPORT OF THE ^{239}PU -> ^{235}U -> ^{231}Pa CHAIN – CONTINUOUS RELEASE

In this section we investigate the transport of the three-member chain ^{239}Pu -> ^{235}U -> ^{231}Pa continuously released from the proposed repository. We study the transport, diffusion and sorption of the members of this chain by means of EOS9nT 3-D site-scale simulations of the entire UZ system of Yucca Mountain. Only mean present-day infiltration was considered in these simulations. The grids, flow fields and conditions were as discussed in the previous section.

The evolution of the mass fractions of the chain members in the release stream at the repository and at

the water table are shown in Figures 9 and 10. Figure 9 reflects decay and generation of the members of the ^{239}Pu chain, and, being a boundary condition, is unaffected by flow or transport conditions in the UZ. Note that the released stream becomes practically devoid of ^{239}Pu due to decay after about 100,000 years, at which time ^{235}U is practically the only species entering the UZ from the repository.

The mass fractions at the water table in Figure 10 incorporate the cumulative effects of migration through the UZ, and reflect the effects of matrix diffusion and sorption. Comparison of Figures 9 and 10 reveals that the radionuclide stream at the water table shows a much earlier enrichment in ^{235}U, which becomes the increasingly dominant species after t = 2,000 years. This is caused by the much stronger sorption of ^{239}Pu, coupled with the relatively weak sorption of ^{235}U. The contribution of ^{231}Pa appears practically insignificant in the first 1,000,000 years.

The inflow-to-outflow relationship is described by the normalized release rate at the water table in Figure 11, computed as the ratio of the total outflow rates (i.e., sum of individual member fluxes) vs. the total inflow rates at the repository. A comparison of Figure 11 to that for ^{239}Pu in Figure 8 (obtained under the same conditions and in the same domain) indicates the importance of considering all the members of the chain in the computations, and the significant error that will be introduced if only the parents are considered. Given the long half life of ^{239}Pu and the much longer half life of ^{235}U, the daughter contributions are very important and cannot be neglected with impunity because of significant radionuclide arrivals are observed at the water table.

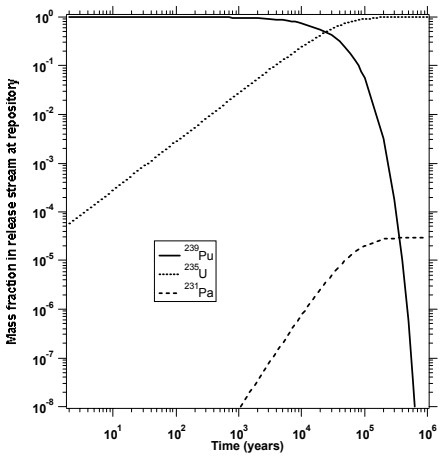

Figure 9. Mass fraction of each member of the ^{239}Pu chain in the release stream at the repository.

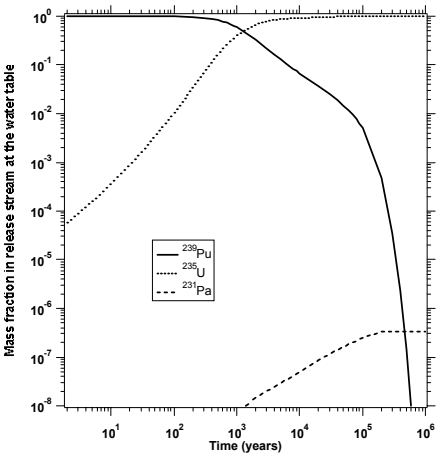

Figure 10. Mass fraction of each member of the ^{239}Pu chain in the release stream at the UZ water table.

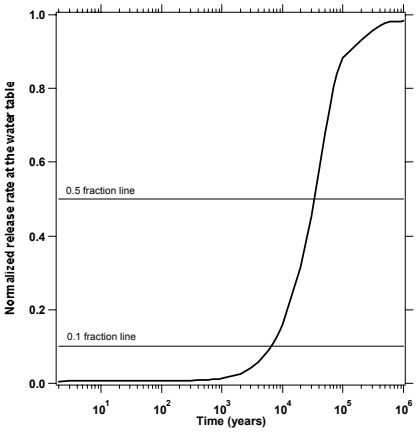

Figure 11. Normalized release rate of the ^{239}Pu chain at the UZ water table (continuous release, mean present-day infiltration).

COLLOID TRANSPORT—CONTINUOUS RELEASE

We investigated the transport of colloids of various sizes (450 nm, 200 nm, 100 nm and 6 nm). Because there are indications that colloid-assisted transport (i.e, transport by pseudocolloids) in the UZ of Yucca Mountain will not be significant because of the low concentrations of naturally occurring colloids such as clays, only true colloids were considered in the simulation. Those were taken to have the properties of PuO_2, and are subject to radioactive decay. In the transport of the colloids, advection, diffusion, dispersion, filtration, and pore-size exclusion were considered. The colloid parameters and properties were as indicated in Moridis et al. (2000).

Three cases were investigated. In Case 1 there is no declogging, with colloids remaining attached on the pore walls after filtration. In Case 2 is the opposite scenario, with a strong kinetic declogging (maximum colloid transport). Case 3 differs from Case 2 in that 1% of the fracture is assumed to be filled with matrix material.

Figure 12 shows the normalized release rate of the four colloids at the water table. For reference, the decaying release rate of the colloids at the repository is included in the figure. Note the very fast breakthrough of the larger colloids (characterized by a rapid rise of the breakthrough curve), all of which have similar behavior. The initial fast riseis followed by a decline caused by decay. Counter to expectations, the smallest colloid (6 nm) exhibits the slowest breakthrough, and never reaches the 0.1 fraction level, indicating that it is sufficiently small to enter the matrix and get attached to the fracture walls.

The colloid behavior is caused by (a) the larger transport velocity of larger colloids, which, by virtue of their size, can only move in the center of pores/fractures where velocities are larger than the average water velocity, and (b) the inability of larger colloids to penetrate into the matrix from the fractures because of low diffusion and size exclusion. Thus, the colloid mass in the fractures is not reduced through colloidal diffusion and/or hydrodynamic dispersion, and practically all of it moves exclusively in the fractures. The 6 nm colloid is capable of diffusing into the matrix, a process which in Figure 12 manifests itself by the substantially slower breakthrough, the very slow and mild rise of the curve, and its low maximum.

Figure 13 shows the relative release rate of the four colloids at the water table in Case 2. The differences between Case 1 and Case 2 are very small, and are most prominent in the case of the 6 nm colloid. The relative insensitivity to the clogging model in the matrix indicates the dominant role of the fractures in the 3-D site scale system, with the matrix appearing to have a minuscule contribution. In Case 3, assigning a porosity of 1% to the fractures, and using the matrix (of Case 2) filtration properties for the fracture describes a fracture with a minor fillup with a porous medium. The results are shown in Figure 14. While the more-freely diffusing 6 nm colloids exhibit a behavior similar to the one in Cases 1 and 2, the occurrence of even a minor fillup retards the transport of the larger colloids.

Additionally, the breakthrough curve assumes a decidedly different shape in the larger colloids, marked by a sudden and dramatic reversal that is consistent in all the three larger colloids. As the occurrence of this phenomenon coincides with the onset of rapid decline in concentrations due to radioactive decay, it is assumed that the kinetic filtration model is very sensitive to minute changes in concentration at this point, hence the sudden slope reversal. However, this issue is not well understood, and will require further investigation.

Note that the significant differences between Figures 12, 13, and 14 are due solely to assigning matrix filtration properties to only 1% of the pore volume of the fractures (by no means an unphysical or unlikely scenario). The significant retardation of the colloids gives a measure of the importance of fractures and their relative contribution to the total colloid transport through the UZ system.

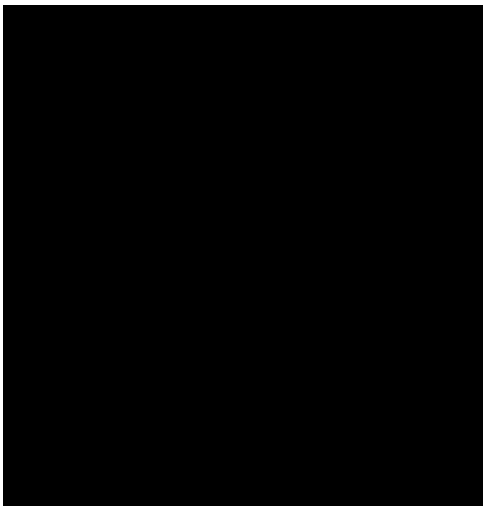

Figure 12. Case 1: Normalized release rate of colloids at the UZ water table (continuous release, mean present-day infiltration).

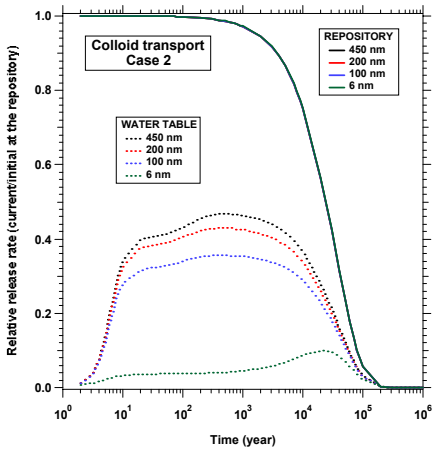

Figure 13. Case 2: Normalized release rate of colloids at the UZ water table (continuous release, mean present-day infiltration).

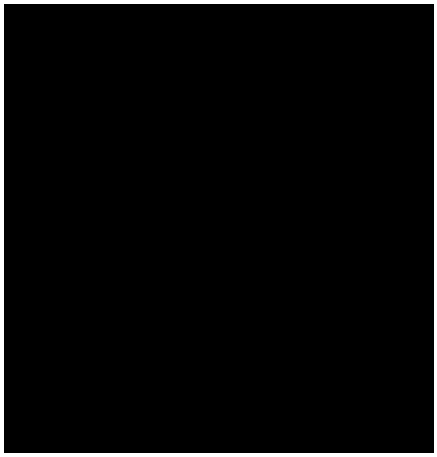

Figure 14. Case 3: Normalized release rate of colloids at the UZ water table (continuous release, mean present-day infiltration).

SUMMARY

The objectives of this study are to evaluate the transport of radioactive solutes and colloids under ambient conditions from the proposed repository horizon at to the water table at YM, and to determine processes and geohydrologic features that significantly affect radionuclide transport. The migration and retardation of radionuclides are analyzed using the T2R3D (Wu et al., 1996) and the EOS9nT codes [Moridis et al., 1999].

Several radionuclides with varying properties are investigated. The results of the study indicate that the most important factors affecting radionuclide transport are the subsurface geology and site hydrology, i.e., the presence of faults (they dominate and control transport), fractures (the main migration pathways), and the relative distribution of zeolitic and vitric tuffs. Diffusion from the fractures into, and subsequent sorption onto, the matrix, are the main retardation processes. Arrival times at the water table increase with the sorption distribution coefficients of the various species, and may have to account for contributions from the decay daughters of certain radionuclides. Increasing infiltration leads to faster transport to the water table. The transport of colloids is strongly influenced by their size (as it affects diffusion into the matrix, straining at hydrogeologic unit interfaces and transport velocity).

ACKNOWLEDGMENT

This work was supported by the Director, Office of Civilian Radioactive Waste Management, U.S. Dept. of Energy, through Memorandum Purchase Order EA9013MC5X between Bechtel SAIC Company, LLC and the Ernest Orlando Lawrence Berkeley National Laboratory (Berkeley Lab). The support is provided to Berkeley Lab through the U.S. Dept. of Energy Contract No. DE-AC03-76SF00098. The authors are grateful to Yvonne Tsang and John Apps for their careful review.

REFERENCES

Bodvarsson, G.S., W. Boyle, R. Patterson, and D. Williams, *Overview of Scientific Investigations at Yucca Mountain - The Potential Repository for High-Level Nuclear Waste*, J. Contam. Hydrol., 38(1–3), 3–24. 1999.

De Hoog, F.R., J.H. Knight, and A.N. Stokes, *An Improved Method for Numerical Inversion of Laplace Transforms*, SIAM J. Sci. Stat. Comput., 3 (3), 357-366, 1982.

Dyer, J.R., and M.D. Voegele, *High-Level Radioactive Waste Management in the United States, Background and Status*, in: Witherspoon, P.A. (Ed.), Geological Problems in Radioactive Waste Isolation, Report LBNL-38915, Lawrence Berkeley National Laboratory, Berkeley, CA, pp. 259-270, 1996.

Hinds, J., and L. Pan, *Development of Numerical Grids for UZ Flow and Transport Modeling*, Report ANL-NBS-HS-000015 Rev. 00, CRWMS M&O, Las Vegas, Nevada, 2000.

Liu, H.H., C.F. Ahlers, and M.A. Cushey, *Analysis of Hydrologic Properties*, Report ANL-NBS-HS-000002 Rev. 00, CRWMS M&O, Las Vegas, Nevada, 2000.

Montazer, P., and W.E. Wilson, *Conceptual Hydrologic Model of Flow in the Unsaturated Zone, Yucca Mountain, Nevada*, Resources Investigations Report 84-4355, U.S. Geological Survey, Denver, Colorado, 1984.

Moridis, G., Y. Wu, and K. Pruess, *EOS9nT: A TOUGH2 Module for the Simulation of Flow and Solute/Colloid Transport*, Report LBNL-42351. Lawrence Berkeley National Laboratory, Berkeley, CA, 1999.

Moridis, G.J., Q. Hu, Y.-S. Wu, and G.S. Bodvarsson, Radionuclide Transport Models Under Ambient Conditions, Report MDL-NBS-HS-000008 Rev. 00, CRWMS M&O, Las Vegas, Nevada, 2000.

Pruess K., *TOUGH2: A General Purpose Numerical Simulator for Multiphase Fluid and Heat Flow*, Report LBL-29400, Lawrence Berkeley Laboratory, Berkeley, CA, 1991.

Wu, Y.S., J. Liu, T. Xu, C. Haukwa, W. Zhang, H.H. Liu, and C.F. Ahlers, UZ Flow Models and Submodels, Report MDL-NBS-HS-000006 Rev. 00, CRWMS M&O, Las Vegas, Nevada, 2000.

Wu, Y.S., C.F. Ahlers, P. Fraser, A. Simmons and K. Pruess, *Software Qualification of Selected TOUGH2 Modules*, *Rep. LBNL-39490*, Lawrence Berkeley Laboratory, Berkeley, CA, 1996.